Optimized state-independent entanglement detection based on a geometrical threshold criterion

Wiesław Laskowski,[1] Christian Schwemmer,[2,3] Daniel Richart,[2,3] Lukas Knips,[2,3] Tomasz Paterek,[4,5] and Harald Weinfurter[2,3]

[1]*Institute of Theoretical Physics and Astrophysics, University of Gdańsk, PL-80-952 Gdańsk, Poland*

[2]*Max-Planck-Institut für Quantenoptik, Hans-Kopfermann-Strasse 1, D-85748 Garching, Germany*

[3]*Department für Physik, Ludwig-Maximilians-Universität, D-80797 München, Germany*

[4]*School of Physical and Mathematical Sciences, Nanyang Technological University, Singapore*

[5]*Centre for Quantum Technologies, National University of Singapore, Singapore*

Experimental procedures are presented for the rapid detection of entanglement of unknown arbitrary quantum states. The methods are based on the entanglement criterion using accessible correlations and the principle of correlation complementarity. Our first scheme essentially establishes the Schmidt decomposition for pure states, with few measurements only and without the need for shared reference frames. The second scheme employs a decision tree to speed up entanglement detection. We analyze the performance of the methods using numerical simulations and verify them experimentally for various states of two, three, and four qubits.

PACS number(s): 03.67.Mn

I. INTRODUCTION

Entanglement is one of the most fundamental features of quantum physics and is considered to be the key resource for quantum information processing [1–3]. In order to detect entanglement, highly efficient witness operators are widely used nowadays [4–10]. However, these operators give conclusive answers only for states close to the target state. To detect entanglement of arbitrary states, positive, but not completely positive, maps [1,4] are the most universal entanglement identifiers. However, they are laborious to use as they require full state tomography. Therefore, more efficient schemes to detect entanglement are most desired.

It has been recently shown that the presence of entanglement in a quantum state is fully characterized by suitable combinations of experimentally accessible correlations and expectation values of local measurements [11]. This enables a simple and practical method to reveal entanglement of all pure states and some mixed states by measuring only few correlations [12]. Since the method is adaptive, it does not require *a priori* knowledge of the state nor a shared reference frame between the possibly remote observers, and thus greatly simplifies the practical application.

Here we extend these results and analyze in detail the possible performance of two schemes for entanglement detection. The first one can be seen as an experimental implementation of Schmidt decomposition, which identifies the maximal correlations through local measurements only. The second scheme shows how to deduce a strategy (decision tree) to find the maximal correlations of an unknown state and obtain a rapid violation of the threshold, identifying entanglement even for an arbitrary number of qubits. The physical principle behind both of our schemes is correlation complementarity [13]. It makes use of trade-offs between correlations present in quantum states. Once a measured correlation is big, other related correlations have to be small, and it is advantageous to move to measurements of the remaining correlations. This simplifies the entanglement detection scheme as a lower number of correlation measurements is required.

II. ENTANGLEMENT CRITERION

A quantum state is entangled if the sum of squared measured correlations exceeds a certain bound [11]. This identifier thus neither requires the measurement of all correlations in a quantum state nor the reconstruction of the density matrix. Rather, it is now the goal to find strategies that minimize the number of correlation measurements. We show how this can be done in different ways described in the subsequent sections. The first method is to identify a Schmidt decomposition from local results and filtering when necessary; the second is a particularly designed decision tree based on correlation complementarity.

Any N-qubit density matrix can be expressed as

$$\rho = \frac{1}{2^N} \sum_{\mu_1,\ldots,\mu_N=0}^{3} T_{\mu_1,\ldots,\mu_N} \sigma_{\mu_1} \otimes \cdots \otimes \sigma_{\mu_N}, \qquad (1)$$

where $\sigma_{\mu_n} \in \{\sigma_0, \sigma_x, \sigma_y, \sigma_z\}$ is the respective local Pauli operator of the nth party (σ_0 being the identity matrix) and the real coefficients $T_{\mu_1,\ldots,\mu_N} \in [-1,1]$ are the components of the correlation tensor $\hat{T}$. They are given by the expectation values of the products of local Pauli observables, $T_{\mu_1,\ldots,\mu_N} = \text{Tr}[\rho(\sigma_{\mu_1} \otimes \cdots \otimes \sigma_{\mu_N})]$, and can be determined by local measurements performed on each qubit.

For N-qubit states, pure or mixed, the following sufficient condition for entanglement holds [11]:

$$\sum_{i_1,\ldots,i_N=1}^{3} T_{i_1,\ldots,i_N}^2 > 1 \Rightarrow \rho \text{ is entangled.} \qquad (2)$$

Note that to prove that a state is entangled, it is sufficient to break the threshold, i.e., in general it is not necessary to measure all correlations. Using fundamental properties of the correlation tensor, we design schemes to minimize the number of required correlation measurements.

III. SCHMIDT DECOMPOSITION

Any pure state of two qubits admits a Schmidt decomposition [14,15],

$$|\psi_S\rangle = \cos\theta|a\rangle|b\rangle + \sin\theta|a_\perp\rangle|b_\perp\rangle, \ \theta \in \left[0, \frac{\pi}{4}\right], \qquad (3)$$

where the local bases $\{|a\rangle, |a_\perp\rangle\}$ and $\{|b\rangle, |b_\perp\rangle\}$ are called the Schmidt bases of Alice and Bob, respectively.

This is an elementary description of bipartite pure quantum states, where the existence of a second term in the decomposition directly indicates entanglement. In addition, in the Schmidt bases, the correlation tensor of a two-qubit state takes a particularly simple form and shows maximal correlations in the state. Therefore, finding the Schmidt bases can be regarded as a redefinition of the measuring operators relative to the state and thus leads to rapid entanglement detection, in at most three subsequent measurements of correlations.

Once the bases are known, Alice constructs her local measurements, $\sigma_{z'} = |a\rangle\langle a| - |a_\perp\rangle\langle a_\perp|$ and $\sigma_{y'} = i|a_\perp\rangle\langle a| - i|a\rangle\langle a_\perp|$, and so does Bob. They can now detect entanglement by using the simple criterion (2) with only two correlation measurements because $T_{z'z'}^2 + T_{y'y'}^2 = 1 + \sin^2 2\theta > 1$ for all pure entangled states. Note that since the bases of Alice and Bob are determined on the fly, the laboratories are not required to share a common reference frame.

In the next sections, we present how to find the Schmidt bases (up to a global phase) from the experimental results gathered on individual qubits. We split the discussion into the two cases of nonvanishing and vanishing Bloch vectors, i.e., local averages (T_{x0}, T_{y0}, T_{z0}), describing the states of the individual qubits.

This systematic procedure to verify entanglement in a pure two-qubit state is represented in Fig. 1, with the sections describing the particular steps.

A. From nonvanishing Bloch vectors to Schmidt bases

Consider first the case of nonzero Bloch vectors. The Schmidt bases of Alice and Bob are related to the standard bases as follows:

$$
\begin{aligned}
|a\rangle &= \cos\xi_A |0\rangle + e^{i\varphi_A}\sin\xi_A |1\rangle, \\
|a_\perp\rangle &= \sin\xi_A |0\rangle - e^{i\varphi_A}\cos\xi_A |1\rangle, \\
|b\rangle &= \cos\xi_B |0\rangle + e^{i\varphi_B}\sin\xi_B |1\rangle, \\
|b_\perp\rangle &= e^{i\delta}(\sin\xi_B |0\rangle - e^{i\varphi_B}\cos\xi_B |1\rangle).
\end{aligned}
\tag{4}
$$

The global phase of $|b_\perp\rangle$ is relevant and required for the characterization of an arbitrary pure state, as can be seen from parameter counting. An arbitrary pure two-qubit state is parametrized by six real numbers (four complex amplitudes minus normalization condition and an irrelevant global phase). By plugging Eqs. (4) into the Schmidt decomposition (3), we indeed find the six relevant real parameters.

Any two-qubit state written in the standard bases of Alice and Bob can be brought into the Schmidt basis of Alice by the transformation

$$
\begin{aligned}
U(\xi_A, \varphi_A) &= |0\rangle\langle a| + |1\rangle\langle a_\perp| \\
&= \cos\xi_A |0\rangle\langle 0| + e^{-i\varphi_A}\sin\xi_A |0\rangle\langle 1| \\
&\quad + \sin\xi_A |1\rangle\langle 0| - e^{-i\varphi_A}\cos\xi_A |1\rangle\langle 1|.
\end{aligned}
\tag{5}
$$

The coefficients ξ_A and φ_A of this transformation can be read from a nonvanishing normalized Bloch vector,

$$
\vec{\alpha} \equiv \frac{\vec{T}^A}{|\vec{T}^A|} = (\sin 2\xi_A \cos\varphi_A, \sin 2\xi_A \sin\varphi_A, \cos 2\xi_A). \tag{6}
$$
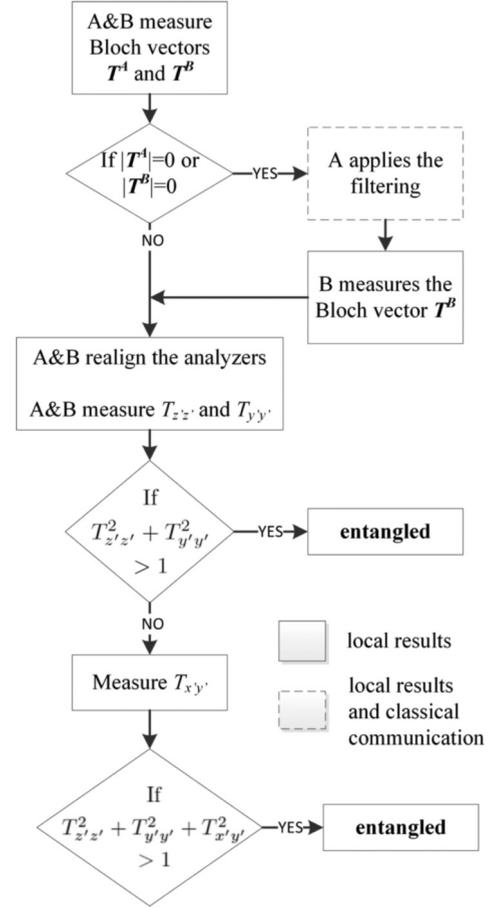
FIG. 1. The systematic way to experimentally verify entanglement of an arbitrary pure two-qubit state without any *a priori* knowledge and in the absence of a common reference frame. The steps of this diagram are described in detail in the main text.

Finally, the coefficients of the Schmidt basis in the standard basis are functions of components of vector $\vec{\alpha} = (T_{x0}, T_{y0}, T_{z0})/\sqrt{T_{x0}^2 + T_{y0}^2 + T_{z0}^2}$ built out of experimentally accessible, local expectation values of Pauli measurements:

$$
\begin{aligned}
\cos\xi_A &= \sqrt{\frac{1+\alpha_z}{2}}, \quad \sin\xi_A = \sqrt{\frac{1-\alpha_z}{2}}, \\
\cos\varphi_A &= \frac{\alpha_x}{\sqrt{1-\alpha_z^2}}, \quad \sin\varphi_A = \frac{\alpha_y}{\sqrt{1-\alpha_z^2}}.
\end{aligned}
\tag{7}
$$

If $T_{z0} = \pm 1$, the standard basis is the Schmidt basis. Note that instead of transforming the state, we can as well transform the measurement operators $\sigma_{n'} = U^\dagger \sigma_n U$. The new operators are given by

$$
\begin{aligned}
\sigma_{x'} &= \frac{-\alpha_x\alpha_z\sigma_x - \alpha_y\alpha_z\sigma_y + (1-\alpha_z^2)\sigma_z}{\sqrt{1-\alpha_z^2}}, \\
\sigma_{y'} &= \frac{\alpha_y\sigma_x + \alpha_x\sigma_y}{\sqrt{1-\alpha_z^2}}, \quad \sigma_{z'} = \alpha_x\sigma_x + \alpha_y\sigma_y + \alpha_z\sigma_z,
\end{aligned}
\tag{8}
$$

and the Schmidt basis is the z' basis, i.e., $\sigma_{z'} = |a\rangle\langle a| - |a_\perp\rangle\langle a_\perp|$.

The equivalent analysis has to be done for the Schmidt basis of Bob. In summary, the Schmidt bases are defined by the direction of the Bloch vectors of the reduced states, up to a

global phase. The global phase of $|b_\perp\rangle$ shows up as a relative phase in the Schmidt decomposition. As it is not obtainable by local measurements, it influences entanglement detection using operators (8).

B. Entanglement detection

Let us denote the basis established by local measurements of Bob by $\{|\tilde{b}\rangle, |\tilde{b}_\perp\rangle\}$, i.e., $|b\rangle = |\tilde{b}\rangle$ and $|b_\perp\rangle = e^{i\delta}|\tilde{b}_\perp\rangle$. Using the locally determined bases, the Schmidt decomposition takes the form

$$|\psi_S\rangle = \cos\theta|a\rangle|\tilde{b}\rangle + e^{i\delta}\sin\theta|a_\perp\rangle|\tilde{b}_\perp\rangle. \tag{9}$$

The correlations that Alice and Bob observe in the measurements related to locally determined bases are $T_{z'z'} = 1$ and $T_{x'x'} = \sin 2\theta \cos\delta$, $T_{y'y'} = -\sin 2\theta \cos\delta$, $T_{x'y'} = \sin 2\theta \sin\delta$, $T_{y'x'} = \sin 2\theta \sin\delta$. Note that the correlation $T_{y'y'}$ would vanish for $\cos\delta = 0$ and the two measurements $T_{z'z'}$ and $T_{y'y'}$ are no longer sufficient (they were sufficient if the full knowledge about the Schmidt bases had been available). In such a case, however, the other two correlations, $T_{x'y'}$ and $T_{y'x'}$, are nonzero and can be used to reveal entanglement. If the first two measurements are not sufficient to overcome the entanglement threshold of (2), then the third measurement of $T_{x'y'}$ correlations will definitely allow exceeding the threshold for every pure entangled state.

C. Vanishing Bloch vectors: Filtering

If the two-qubit state is maximally entangled, i.e., in the Schmidt decomposition $|\kappa\rangle = \frac{1}{\sqrt{2}}(|a\rangle|b\rangle + |a_\perp\rangle|b_\perp\rangle)$, then the Bloch vector is of zero length, $|\vec{T}^A| = 0$, and the whole system admits infinitely many Schmidt decompositions. For every unitary operation of Alice, U, there exists an operation of Bob, U', such that the state is unchanged,

$$U \otimes U'|\kappa\rangle = |\kappa\rangle. \tag{10}$$

Therefore, any basis of, say, Alice can serve as the Schmidt basis as soon as we accordingly update the basis of Bob. Our strategy to reveal the corresponding basis of Bob is to filter in the chosen Schmidt basis of Alice. It is best to explain it with an example. Assume Alice chooses the standard basis as her Schmidt basis. Due to the mentioned invariance of the maximally entangled state, there exists a Schmidt basis of Bob such that

$$|\kappa\rangle = \frac{1}{\sqrt{2}}(|0\rangle|b'\rangle + |1\rangle|b'_\perp\rangle). \tag{11}$$

The basis of Bob can be found by the filtering of Alice, $F = \varepsilon|0\rangle\langle 0| + |1\rangle\langle 1|$ with $\varepsilon \in [0,1)$. We implemented this operation experimentally and provide the details later. In short, we use devices which are transparent to the $|1\rangle$ state, but probabilistically "reflect" the $|0\rangle$ state. If we imagine that a perfect detector is observing a port of this device where the reflected particle travels, and we see no detection, the filter operation is performed on the initial state. If Alice applies the filtering on her qubit and informs Bob that the filtering was successful, the initial state becomes

$$(F \otimes \mathbb{1})|\kappa\rangle \to \frac{1}{\sqrt{1 + \varepsilon^2}}(\varepsilon|0\rangle|b'\rangle + |1\rangle|b'_\perp\rangle). \tag{12}$$

The result of filtering is that for Bob, a Bloch vector emerges and we can again use the method described above to find his Schmidt basis.

D. Performance

Summing up all required steps, we see that to experimentally verify entanglement of any pure two-qubit state without any further *a priori* knowledge requires at least 2×3 local measurements to determine the Schmidt bases and, sometimes, filtering requiring three local measurements more. Finally, two more (or three if $\delta = \pi/2$) correlation measurements allow one to verify the entanglement criterion.

IV. DECISION TREE

Our second algorithm for entanglement detection does not even require any initial measurements and directly applies also to mixed states. We will split the presentation into bipartite and multipartite cases. The decision tree provides an adaptive method to infer the next measurement setting from previous results.

A. Two qubits

Alice and Bob choose three orthogonal local directions x, y, and z independently from each other and agree to only measure correlations along these directions. In Fig. 2, we show exemplarily which correlations should be measured in order to detect entanglement in a small number of steps. Starting with a measurement of T_{zz}, one continues along the solid (dotted) arrow, if the correlation is higher (lower) than some threshold value t. We performed detailed numerical analysis on how the efficiency of entanglement detection depends on the threshold value. The efficiency is quantified by the percentage of entangled states detected at various steps of the decision
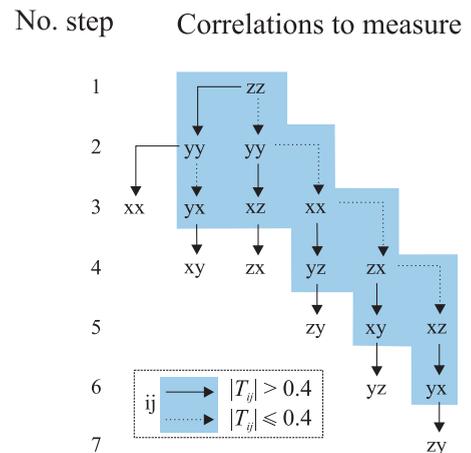
FIG. 2. (Color online) Decision strategies to detect entanglement. Start with a measurement of the correlation T_{zz} and proceed with the correlation along the solid (dotted) arrow if the measured correlation is higher (lower) than the chosen threshold value; here of $t = 0.4$. Due to correlation complementarity, there is a good chance of detecting entanglement in a small number of steps. The measurements in the blue shaded area suffice to detect all maximally entangled pure states with Schmidt-basis vectors x, y, or z.

tree. It turns out that the efficiency does not depend much on the threshold value and the best results are obtained for $t = 0.4$. We therefore set this threshold value in all of our simulations.

The construction of the tree is based on the principle of correlation complementarity [13,16–18]: in quantum mechanics, there exist trade-offs for the knowledge of dichotomic observables with corresponding anticommuting operators. For this reason, if the correlation $|T_{zz}|$ is big, then correlations $|T_{zx}|, |T_{zy}|, |T_{xz}|$, and $|T_{yz}|$ have to be small because their corresponding operators anticommute with the operator $\sigma_z \otimes \sigma_z$. Therefore, the next significant correlations have to lie in the xy plane of the correlation tensor and the next step in the tree is to measure the T_{yy} correlation.

In cases in which going through the whole tree did not reveal entanglement, we augmented it with additional measurements of correlations that were not established until that moment. The order of the additional measurements also results from the correlation complementarity. With every remaining measurement, we associate the "priority" parameter

$$P_{ij} = \sum_{k \neq i} P_{ij}(T_{kj}) + \sum_{l \neq j} P_{ij}(T_{il}), \quad (13)$$

which depends on the measurements of the decision tree in the following way:

$$P_{ij}(T_{mn}) = \begin{cases} T_{mn}^2 & \text{if } T_{mn} \text{ was performed before,} \\ 0 & \text{otherwise.} \end{cases} \quad (14)$$

According to the correlation complementarity, if the value of the corresponding parameter is small, there is a bigger chance that this correlation is significant. Therefore, the correlations T_{ij} with lower values of P_{ij} are measured first.

Let us illustrate this with the following example. The measured correlations of the decision tree are as follows: $T_{zz} = 0.7$, $T_{yy} = 0.6$, and $T_{xx} = 0.1$. Therefore, $P_{xy} = P_{yx} = T_{xx}^2 + T_{yy}^2 = 0.37$, $P_{xz} = P_{zx} = T_{xx}^2 + T_{zz}^2 = 0.5$, and $P_{yz} = P_{zy} = T_{zz}^2 + T_{yy}^2 = 0.85$. Accordingly, the order of the remaining measurements is as follows: first measure xy, then yx, and next xz, zx, yz, and zy.

B. Many qubits

Correlation complementarity, which holds also in the multipartite case, states that for a set $\{\alpha_1, \ldots, \alpha_k\}$ of dichotomic mutually anticommuting multiparty operators, the following trade-off relation is satisfied by all physical states:

$$T_{\alpha_1}^2 + \cdots + T_{\alpha_k}^2 \leqslant 1, \quad (15)$$

where T_{α_1} is the expectation value of observable α_1, and so on. Therefore, if one of the expectation values is maximal, say $T_{\alpha_1} = \pm 1$, then the other anticommuting observables have vanishing expectation values and do not have to be measured. In this way, we exclude exponentially many, in number of qubits, potential measurements because that many operators anticommute with α_1, and we apply correlation complementarity pairwise to α_1 and one of the anticommuting operators. This motivates taking only sets of commuting operators along the branches of the decision tree that should be followed if the measured correlations are big.

We are thus led to propose the following algorithm generating one branch of the decision tree in which the first measurement, called $X \otimes X \otimes \cdots \otimes X$, is assumed to have a big expectation value.

(i) Generate all N-partite Pauli operators that commute with $X \otimes X \otimes \cdots \otimes X$.

Such operators have an even number of local Pauli operators different than X. Accordingly, their number is given by $\sum_{j=1}^{\lfloor \frac{N}{2} \rfloor} 2^{2j} \binom{N}{2j} = \frac{1}{2}(3^N - 1) - \text{Odd}(N)$, where $\text{Odd}(N) = 1$ if N is odd, and 0 otherwise. For example, in the three-qubit case, the set of operators commuting with XXX consists of 12 operators: XZZ, ZZX, ZXZ, XYY, YYX, YXY, XYZ, XZY, YXZ, YZX, ZXY, and ZYX.

(ii) Group them in strings of mutually commuting operators that contain as many elements as possible.

We verified for N up to eight qubits (and conjecture, in general) that the length of the string of mutually commuting operators is $L = 2^{N-1} + \text{Even}(N)$, where $\text{Even}(N) = 1$ if N is even, and 0 otherwise. In our three-qubit example, we have the following strings: $\{XXX, YXZ, XZZ, YZX\}$, $\{XXX, YYX, XYZ, YXZ\}$. $\{XXX, XZY, YZX, YXY\}$, $\{XXX, XZZ, ZXZ, ZZX\}$, $\{XXX, XYZ, ZXZ, ZYX\}$, $\{XXX, YXY, YYX, XYY\}$, $\{XXX, XYY, ZXY, ZYX\}$, and $\{XXX, ZZX, XZY, ZXY\}$. We denote the number of such strings by M.

(iii) Arrange the operators within the strings and sort the strings such that they are ordered with the same operator in the first position, then, if possible, second, third, etc.

In this way, we produce a set of strings $\{S_1, S_2, \ldots, S_M\}$ such that in the first position of every string, we have $S_{j,1} = X \otimes X \otimes \cdots \otimes X$; in the second position, the number of different operators is smaller or equal to the number of different operators in the third position, etc. After applying that operation in the three-qubit example, we obtain $\{XXX, XZZ, ZXZ, ZZX\}$, $\{XXX, XZZ, YXZ, YZX\}$, $\{XXX, XZY, YZX, YXY\}$, $\{XXX, XZY, ZZX, ZXY\}$, $\{XXX, XYZ, YXZ, YYX\}$, $\{XXX, XYZ, ZXZ, ZYX\}$, $\{XXX, XYY, YXY, YYX\}$, and $\{XXX, XYY, ZXY, ZYX\}$.

(iv) Connect the operators of the string S_1 with continuous arrows,

$$S_{1,1} \longrightarrow S_{1,2} \longrightarrow \cdots \longrightarrow S_{1,L}. \quad (16)$$

(v) For all other strings S_j, with $j = 2, \ldots, M$, check on which position string S_j differs from S_{j-1}. Let us denote this position by d. At these positions, strings are connected with another type of arrow, yielding the tree as

$$S_{j-1,d} \dashrightarrow S_{j,d} \longrightarrow S_{j,d+1} \longrightarrow \cdots \longrightarrow S_{j,L}. \quad (17)$$

By using the strings of operators from step (iii) and choosing some threshold as to whether to follow one or the other string, we can now build up a decision tree, as shown in Fig. 3. Its essential feature is that an operator with big expectation value is followed only by the measurements of commuting operators, irrespectively of their expectation values.
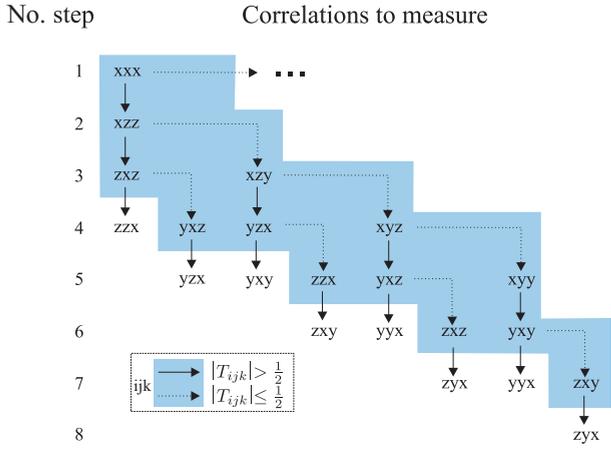
FIG. 3. (Color online) One branch of the decision tree for three qubits, starting with a measurement of the correlation T_{xxx} assumed to be big. The best efficiency is obtained for the threshold $t = 0.5$.

C. Bloch correlations

Finally, it would be useful to establish a measurement suitable as a starting point of the decision tree, i.e., such that the measured correlations have a good chance of being big. A natural candidate is to connect both methods discussed here and check whether the correlation measured along the Bloch vectors of every observer (we denote it as Bloch correlations) gives values close to the maximal correlation in a pure state. We verified this numerically and found that the Bloch correlations are larger than $\frac{3}{4}$ of maximal correlations in a pure state in 100% of two-qubit states and 69% of three-qubit states, but only in 27% of four-qubit states and 3% of five-qubit states. Therefore, the Bloch correlations give a very good starting point of the decision tree only for two and three qubits. We leave it as an open question whether a simple and reliable method exists that identifies the maximal correlations of a pure multiqubit state.

D. Performance

Let us analyze the results on the entanglement detection efficiency for different classes of two-qubit states. As explained in Sec. III B, at maximum, three correlation measurements are sufficient to detect entanglement once the local Schmidt bases of Alice and Bob are known. Here, in contrast, we study how many correlation measurements are needed when the decision tree is applied to an unknown entangled state.

The dependence of the efficiency of the algorithm on the number of steps involved can be seen in Fig. 4. The efficiency is defined by the fraction of detected entangled states with respect to all randomly generated entangled states. For nine steps, the algorithm detects all pure entangled states. This is expected because Eq. (2) is a necessary and sufficient condition for entanglement in the case of pure states. In the case of mixed states, Fig. 4 shows how the efficiency of the algorithm scales with the purity of the tested state. Since condition (2) is similar to the purity of a state, obviously, the scheme succeeds the faster a state becomes more pure.

Figure 4 also shows that the efficiency of the decision tree grows with the amount of entanglement in a state as
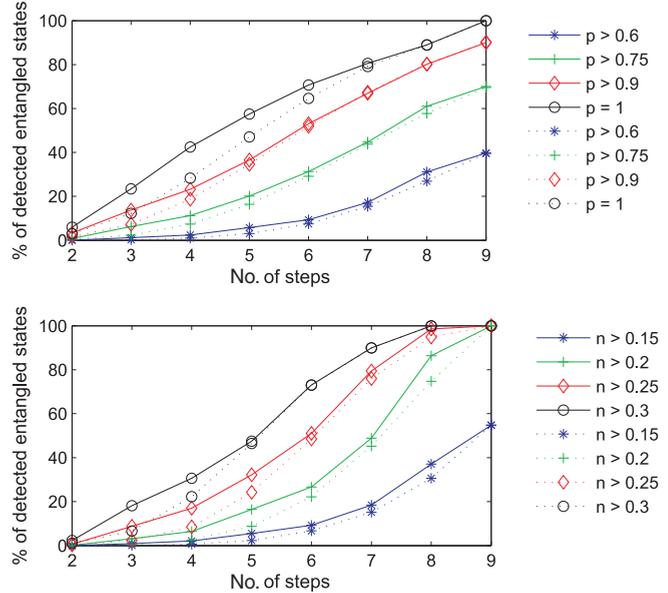
FIG. 4. (Color online) Efficiency of the decision tree for two-qubit random mixed states. The states were uniformly sampled according to the Haar measure. The efficiency increases with the purity of the state (top panel) as well as with the amount of entanglement in a tested state (bottom panel). Note that all pure entangled states are detected after nine steps, as well as all the states with negativity of more than 0.2 independently of their purity. Solid lines show the results when using the decision tree; dotted lines show the results when using random choices for the measurements.

characterized by the negativity [19]. It turns out that the tree detects all the states that have negativity of more than $\frac{1}{5}$.

We also compared the efficiency of the decision tree algorithm to entanglement detection based on a random order of measurements. In the first step of this protocol, Alice and Bob randomly choose one of nine measurements that also enter the decision tree. In the second step, they randomly measure one of the eight remaining measurements, and so on. At each step, condition (2) is checked for entanglement detection. Of course, the two methods converge for higher number of measurements. For a small number of measurements, the decision tree detects entanglement roughly one step faster than the random-measurement method. The advantage of the decision tree with respect to a random choice of the correlations is more pronounced for a higher number of qubits (see Sec. IV D3).

Condition (2) alone, i.e., without considering specific, state-dependent metrics (see [11]), cannot detect all mixed entangled states. As an illustration of how the decision tree works for mixed states, we first consider Werner states. It turns out that not all entangled states of this family can be detected, whereas the following example shows a family of mixed states for which all of the states are detected.

1. Werner states

Consider the family of states

$$\rho = p|\psi^-\rangle\langle\psi^-| + (1-p)\frac{1}{4}\mathbb{1}, \qquad (18)$$

where $|\psi^-\rangle = \frac{1}{\sqrt{2}}(|01\rangle - |10\rangle)$ is the Bell singlet state, $\frac{1}{4}\mathbb{1}$ describes the completely mixed state (white noise), and p is

a probability [20]. Its correlation tensor, written in the same coordinate system for Alice and Bob, is diagonal with entries $T_{xx} = T_{yy} = T_{zz} = -p$, arising from the contribution of the entangled state. The states (18) are entangled if and only if $p > \frac{1}{3}$, whereas the decision tree reveals the entanglement only for $p > \frac{1}{\sqrt{3}} \approx 0.577$.

2. Entanglement mixed with colored noise

An exemplary class of density operators for which the decision tree detects all entangled states is provided by

$$\gamma = p|\psi^-\rangle\langle\psi^-| + (1-p)|01\rangle\langle01|, \tag{19}$$

i.e., the maximally entangled state is mixed with colored noise $|01\rangle$ bringing anticorrelations along the local z axes. For this case, quite common for type-II parametric down-conversion sources, we obtain the following nonvanishing elements of its correlation tensor: $T_{xx} = T_{yy} = -p$ and $T_{zz} = -1$. Therefore, the decision tree allows detection of entanglement in this class of states in two steps. Note that the state is entangled already for an infinitesimal admixture of the Bell singlet state. We also verified numerically that for a hundred random choices of local coordinate systems, the decision tree detects entanglement even for $p > 10^{-3}$.

3. Three and more qubits

Similarly to the two-qubit case, we also studied the efficiency of the three-qubit decision tree of Fig. 3, as well as similar trees for higher number of qubits. The results for three qubits are presented in Fig. 5 and reveal that the decision tree is roughly two steps ahead of the protocol with a random order of measurements for small number of steps. In general, the number of steps the decision tree is ahead of the protocol with a random order of measurements grows exponentially with the number of qubits (see Fig. 6). The intuition behind this is that once big correlations are measured using the decision tree, a set of measurements exponential in size is excluded, whereas these measurements would still be randomly sampled in the other protocol.
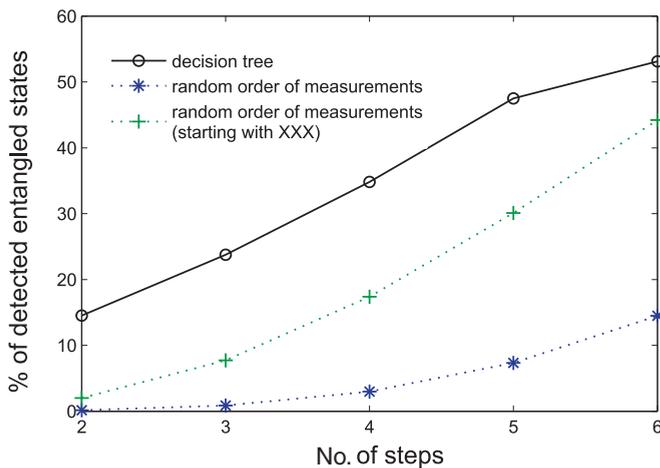
FIG. 5. (Color online) Efficiency of one branch of the decision tree for three-qubit random pure states. The states were uniformly sampled according to the Haar measure.
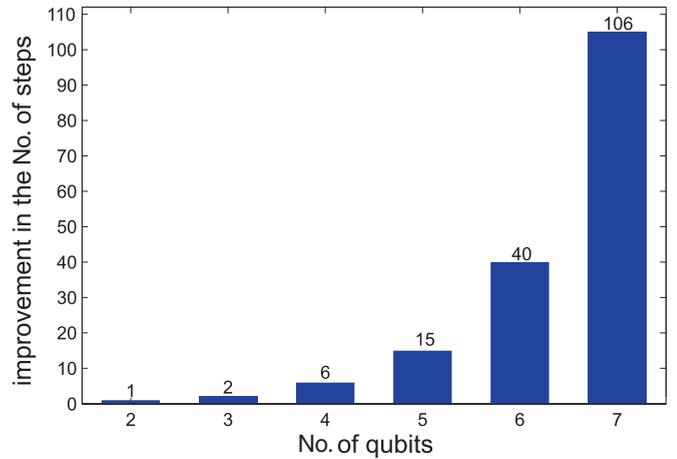
FIG. 6. (Color online) Efficiency of one branch of the decision tree for many qubits compared with a random choice of measurements. The plot shows the gain in the number of measurements provided by the decision tree. Pure states were uniformly sampled according to the Haar measure and the percentage of detected entangled states was calculated for different number of steps (measurements) in the tree as well as for the random order of measurements that start with $X \otimes \cdots \otimes X$ for a fair comparison. We then compare the number of measurements for which the percentage of detected entangled states using the decision tree is the same as using the randomized measurements and plot here the maximal difference between them. The improvement provided by the tree grows exponentially with the number of qubits.

V. EXPERIMENTS

The entanglement detection schemes introduced above are experimentally evaluated by analyzing a variety of multiqubit entangled states. These states were created by spontaneous parametric down conversion (SPDC). Here, for the preparation of two-qubit entangled states, a type-I source with two crossed optically contacted β-barium-borate (BBO) crystals of 1 mm thickness is used; see Fig. 7 [21]. The computational basis $|0\rangle$ and $|1\rangle$ as introduced before is encoded in the polarization state $|H\rangle$ and $|V\rangle$, respectively. A continuous-wave laser diode (Nichia Corporation) at 402 nm is used to pump the BBO crystals with approximately 60 mW. The polarization of the
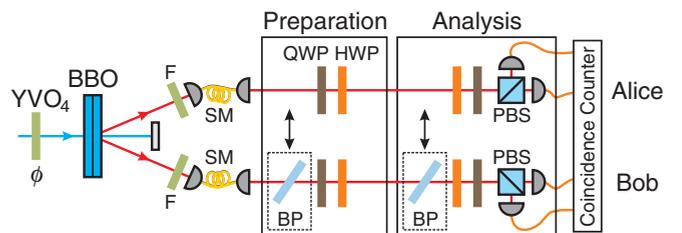
FIG. 7. (Color online) Scheme of the experimental type-I SPDC source used to prepare the state $\frac{1}{\sqrt{2}}(|HH\rangle + e^{i\phi}|VV\rangle)$. The phase ϕ can be set by an yttrium-vanadate crystal (YVO$_4$). Spectral filtering is performed by means of interference filters (F) and spatial filtering by single mode fibers (SM). Half- (HWP) and quarter-wave plates (QWP) are used for state preparation and analysis. Brewster plates (BP) enable the performance of the filter operation and the preparation of asymmetric states.

pump light is oriented at 45°, allowing one to equally pump both crystals and to emit HH and VV polarized photon pairs with the same probability. However, a delay longer than the pump photon coherence length is acquired between the photon pairs generated in the first or second crystal over the length of the crystals, reducing their temporal indistinguishability. Therefore, an yttrium-vanadate (YVO$_4$) crystal of 200 μm thickness is introduced in front of the BBOs to precompensate for the delay and to set the phase ϕ between HH and VV. Using this configuration, entangled states of the form $|\Psi\rangle = \frac{1}{\sqrt{2}}(|H\rangle|H\rangle + e^{i\phi}|V\rangle|V\rangle)$ are generated [22].

In order to reduce the spectral bandwidth of the photon pairs, interference filters centered at 805 nm with a bandwidth of 7 nm are used. Spatial filtering is accomplished by coupling the photons at corresponding points of their emission cones into a pair of single-mode fibers. Polarization controllers allow for the compensation of the polarization rotation of the fibers. Then, the photons are transmitted through a set of quarter- (QWP) and half-wave plates (HWP), allowing an arbitrary transformation of the polarization state in each path. A set of Brewster plates with a loss rate up to $\approx$60% for V and high transmission for H polarized light can be introduced in front of the wave plates to enable preparation of states. For the analysis, both Alice and Bob are provided with HWP and QWP as well as a filter (another Brewster plate) for Bob. Photons are then projected onto $|H\rangle$ and $|V\rangle$ implemented by a polarizing beam splitter (PBS) and respective detectors. Note that local filtering can also be accomplished by a polarizer. The output modes of the analyzing PBS are coupled into multimode fibers connected to avalanche photon detectors (SPCM-AQ4C, Perkin-Elmer module) with a photon detection efficiency of $\approx$50%. A coincidence logic is applied to extract the respective coincidence count rates within a time accuracy of <10 ns. The observed coincidence rate is approximately 200 s^{-1} and a measurement time of 10 s per basis setting allows one to register about 2000 events.

A. Schmidt decomposition

In order to perform the measurement in the Schmidt basis, we first have to determine basis vectors from the Bloch vectors observed by Alice and Bob. Let us consider the state depicted in Fig. 8(a). The table to the left shows the correlation tensor elements T_{ij} with the Bloch vectors of Alice (Bob) in the leftmost column (top row). For the application of the Schmidt decomposition method, Alice and Bob measure first their respective Bloch vectors (measurements actually to be performed are indicated by the blue shaded fields). Since they are close to 0, $\vec{T}_A = (0.002, 0.043, 0.017)$ and $\vec{T}_B = (0.109, -0.029, 0.029)$, the next step of the algorithm is to apply local filtering, as described by the scheme of Fig. 1. The filtered state shown in Fig. 8(b) has nonvanishing Bloch vectors, $\vec{T}_A = (0.338, -0.186, -0.136)$ and $\vec{T}_B = (-0.074, 0.147, 0.299)$, which can be used to find the corresponding Schmidt basis of the shared two-qubit state.[1]

---

[1]It should be noted that the Bloch vectors are determined from coincidence measurements. This is due to the low detection efficiency of correlated photons.

(a) Initial state

1	B	X	Y	Z
1	A	0.002	0.043	0.017
X	0.109	0.665	0.225	0.599
Y	−0.029	0.442	0.640	−0.570
Z	0.029	0.615	−0.649	−0.350

Re(ρ)

(b) Filtering

1	B	X	Y	Z
1	A	−0.074	0.147	0.299
X	0.338	0.518	0.220	0.646
Y	−0.186	0.393	0.522	−0.577
Z	−0.136	0.587	−0.603	−0.310

Re(ρ)

(c) Schmidt decomposition

1	B	X′	Y′	Z′
1	A	−0.015	−0.002	−0.035
X′	0.024	−0.946	−0.170	−0.195
Y′	−0.017	0.126	−0.906	−0.237
Z′	0.042	0.153	0.250	−0.919

Re(ρ)
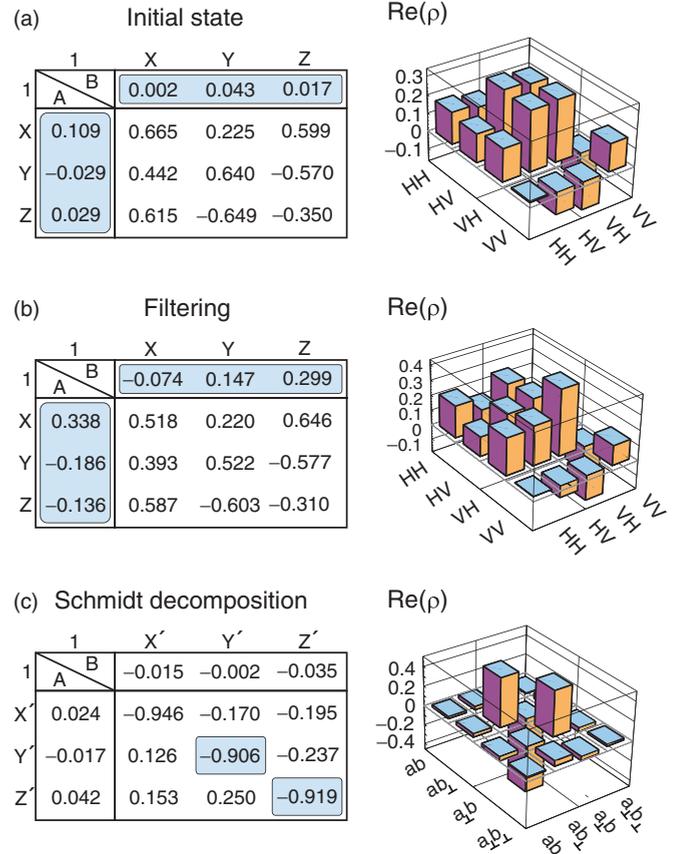
FIG. 8. (Color online) Schmidt decomposition of a maximally entangled unknown state. The correlation tensor and the density matrix are determined (a) before and (b) after applying local filtering. (c) After removing the filter, the state can be measured in its Schmidt basis.

If the phase ϕ is not determined by an additional correlation measurement, there are infinitely many such bases. As shown in Sec. III A, one possible choice is to redefine the local basis of Alice and Bob according to Eq. (8). Measuring along $\sigma_{i'}$ corresponds to a projection on its eigenstates $|\downarrow\rangle_{i'}$ and $|\uparrow\rangle_{i'}$. The task now is to find the angles for the wave plates of Alice and Bob, $\theta_A^{i'}/\phi_A^{i'}$ and $\theta_B^{i'}/\phi_B^{i'}$, respectively. Since the PBS of the polarization analysis shown in Fig. 9 always projects on $|H\rangle$ and $|V\rangle$, the angles are calculated under the condition that $|\downarrow\rangle_{i'}$ ($|\uparrow\rangle_{i'}$) is rotated, up to a global phase τ, to $|H\rangle$ ($|V\rangle$), e.g.,
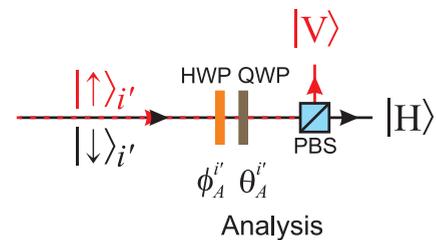
FIG. 9. (Color online) If Alice wants to measure in the basis $\sigma_{i'} = |\downarrow\rangle_{i'}\langle\downarrow|_{i'} - |\uparrow\rangle_{i'}\langle\uparrow|_{i'}$ ($i = x,y,x$), then the HWP and the QWP of the polarization analysis have to be aligned such that $|\downarrow\rangle_{i'}$ and $|\uparrow\rangle_{i'}$ are detected at different outputs of the PBS. The same holds for Bob.

TABLE I. Wave-plate settings for Alice and Bob to measure the maximally entangled state shown in Fig. 8(a) in the Schmidt basis and the complementary directions.

	Alice			Bob	
	$\frac{\lambda}{2}$	$\frac{\lambda}{4}$		$\frac{\lambda}{2}$	$\frac{\lambda}{4}$
$\sigma_{x'}$	22.6°	25.8°	$\sigma_{x'}$	6.6°	4.6°
$\sigma_{y'}$	−15.8°	13.3°	$\sigma_{y'}$	7.2°	−30.6°
$\sigma_{z'}$	−9.9°	−12.8°	$\sigma_{z'}$	34.7°	13.5°

TABLE II. Wave-plate settings for Alice and Bob to measure the asymmetric state shown in Fig. 10(a) in the Schmidt basis and the complementary directions.

	Alice			Bob	
	$\frac{\lambda}{2}$	$\frac{\lambda}{4}$		$\frac{\lambda}{2}$	$\frac{\lambda}{4}$
$\sigma_{x'}$	0.7°	0.8°	$\sigma_{x'}$	21.9°	9.4°
$\sigma_{y'}$	−13.5°	17.9°	$\sigma_{y'}$	40.0°	−55.0°
$\sigma_{z'}$	−35.2°	−27.0°	$\sigma_{z'}$	42.0°	3.3°

for Alice

$$U_{\mathrm{QWP}}(\theta_A^{i'})U_{\mathrm{HWP}}(\phi_A^{i'})|\downarrow\rangle_{i'} = e^{i\tau_1}|H\rangle, \qquad (20)$$

$$U_{\mathrm{QWP}}(\theta_A^{i'})U_{\mathrm{HWP}}(\phi_A^{i'})|\uparrow\rangle_{i'} = e^{i\tau_2}|V\rangle, \qquad (21)$$

where U labels the unitary operation of the corresponding wave plate. The angles $\theta_A^{i'}/\phi_A^{i'}$ and $\theta_B^{i'}/\phi_B^{i'}$ can be found by (numerically) solving the equation

$$\left|\langle H|U_{\mathrm{QWP}}(\theta_A^{i'})U_{\mathrm{HWP}}(\phi_A^{i'})|\downarrow\rangle_{i'}\right|^2 = 1, \qquad (22)$$

and similarly for Bob. Using this scheme, we find the angles for Alice's and Bob's wave plates, such that their qubits are measured in the primed bases, presented in Table I.

After removing the filter, Alice and Bob can now measure in their new bases and reveal entanglement by measuring $T_{z'z'}$, followed by $T_{y'y'}$, and possibly $T_{y'x'}$. Here, the two measurements suffice to reveal entanglement as $T_{z'z'}^2 + T_{y'y'}^2 = 1.665 \pm 0.05 > 1$.

In full analogy to the previous example, it is also possible to apply the Schmidt decomposition scheme to a nonmaximally entangled state, e.g., as presented in Fig. 10(a). For using the Schmidt decomposition strategy, first both parties agree on measuring their respective Bloch vectors, $\vec{T}_A =$

(0.072, −0.026, −0.213) and $\vec{T}_B = (-0.201, 0.279, 0.012)$. As they already can be distinguished from noise, Alice and Bob can find the Schmidt bases without applying the filter operation. The angle settings of the wave plates for analyzing in the Schmidt bases are again calculated using (22) and are shown in Table II. Again, the state is proved to be entangled after only two correlation measurements since $T_{z'z'}^2 + T_{y'y'}^2 = 1.624 \pm 0.047 > 1$; see Fig 10(b).

B. Decision tree

1. Two qubits

Let us first consider the two states analyzed above using Schmidt decomposition. For the first state (Fig. 8), we see that a direct application of the decision tree shown in Fig. 2 would require four correlation measurements to reveal entanglement, namely, $T_{zz}^2 + T_{yy}^2 + T_{xz}^2 + T_{zx}^2 = (-0.350)^2 + 0.640^2 + 0.599^2 + 0.615^2 = 1.33 \pm 0.03 > 1$. Similarly, the analysis of the second state (Fig. 10) would require four correlation measurements to determine entanglement, namely, $T_{zz}^2 + T_{yy}^2 + T_{xx}^2 + T_{xz}^2 = (-0.312)^2 + 0.582^2 + 0.579^2 + 0.622^2 = 1.158 \pm 0.030 > 1$. This shows that quite a few more correlation measurements are needed when using the decision tree. Yet, it saves measuring the Bloch vectors and filtering operations. To illustrate the entanglement detection scheme, we further apply it to a selection of maximally entangled states (Fig. 11) and to nonmaximally entangled states (Fig. 12).

For didactical reasons, the full correlation tensors are depicted, in both cases. In order to reveal entanglement, the decision tree requires the measurement of a number of correlations much smaller than needed to reconstruct the full density matrix. Following the lines as described in Sec. IV, only correlation measurements shaded red are required to detect entanglement. As an example, let us consider the state $\frac{1}{\sqrt{2}}(|RR\rangle + |LL\rangle)$ [Fig. 11(g)], for which a measurement of the two correlations $T_{zz} = 0.905$ and $T_{yy} = 0.977$ suffices to reveal entanglement since $T_{zz}^2 + T_{yy}^2 = 1.773 \pm 0.039 > 1$. In contrast, for the state $\frac{1}{\sqrt{2}}(|RP\rangle + i|LM\rangle)$ [Fig. 11(e)], the algorithm only stops after six steps, as the measurements of $T_{zz} = -0.089$, $T_{yy} = -0.091$, $T_{xx} = 0.099$, $T_{zx} = -0.194$, $T_{xz} = 0.941$, and $T_{yx} = 0.961$ are required to beat the threshold, i.e., $1.872 \pm 0.058 > 1$. A similar reasoning is applied to reveal entanglement of other two-qubit states.

The entanglement detection scheme is further applied to a selection of nonmaximally entangled states (Fig. 12). As an example, let us consider the state $0.83|LH\rangle + 0.56i|RV\rangle$

(a) Initial state

1		X	Y	Z
1	B A	−0.201	0.279	0.012
X	0.072	0.579	0.224	0.622
Y	−0.026	0.431	0.582	−0.571
Z	−0.213	0.638	−0.681	−0.312

(b) Schmidt decomposition

1		X′	Y′	Z′
1	B A	0.006	0.103	−0.326
X′	−0.045	−0.902	0.268	0.049
Y′	−0.025	−0.311	−0.852	−0.145
Z′	0.286	0.002	0.186	−0.948
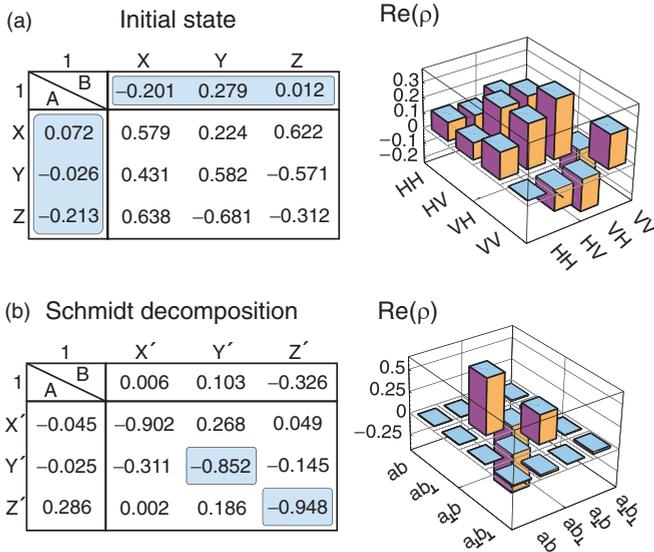
FIG. 10. (Color online) Schmidt decomposition of a nonmaximally entangled state. (a) The correlation tensor and density matrix are displayed for an unknown asymmetric state. (b) The state has nonzero Bloch vectors enabling one to determine the corresponding Schmidt basis for which the measured correlations are maximal.

(a) $(|HH\rangle + |VV\rangle)/\sqrt{2}$

A\B	1	X	Y	Z
1		−0.114	0.024	0.052
X	−0.101	0.969	−0.023	0.058
Y	−0.023	−0.013	−0.949	−0.061
Z	0.071	−0.073	−0.008	0.984

after filtering
−0.034	−0.045	0.401	B
−0.031	−0.033	0.422	A

Σ 1.869+/−0.029>1
Σ 1.869+/−0.029>1

(b) $(|PP\rangle + i|MM\rangle)/\sqrt{2}$

A\B	1	X	Y	Z
1		−0.087	−0.067	0.002
X	−0.062	0.951	−0.074	−0.164
Y	0.045	−0.242	−0.131	−0.933
Z	−0.046	−0.113	−0.954	0.053

after filtering
−0.084	0.091	0.371	B
−0.151	0.306	0.084	A

Σ 1.794+/−0.046>1
Σ 1.780+/−0.044>1

(c) $(|RH\rangle - i|LV\rangle)/\sqrt{2}$

A\B	1	X	Y	Z
1		0.064	0.027	0.022
X	−0.080	−0.942	−0.229	0.053
Y	0.042	0.039	−0.190	0.959
Z	−0.023	0.083	−0.915	−0.204

after filtering
−0.057	−0.034	0.371	B
0.086	0.280	0.066	A

Σ 1.884+/−0.049>1
Σ 1.859+/−0.046>1

(d) $(|PP\rangle - |MM\rangle)/\sqrt{2}$

A\B	1	X	Y	Z
1		0.010	0.031	−0.068
X	0.013	0.978	0.088	−0.072
Y	0.034	0.048	0.945	0.067
Z	0.047	−0.062	0.106	−0.933

after filtering
−0.079	0.001	0.460	B
−0.110	0.088	−0.454	A

Σ 1.763+/−0.036>1
Σ 1.763+/−0.036>1

(e) $(|RP\rangle + i|LM\rangle)/\sqrt{2}$

A\B	1	X	Y	Z
1		0.018	−0.010	−0.040
X	0.054	0.099	−0.082	0.941
Y	−0.057	0.961	−0.091	−0.054
Z	0.082	−0.194	−0.936	−0.089

after filtering
−0.012	−0.030	0.424	B
0.354	0.104	0.089	A

Σ 1.872+/−0.058>1
Σ 1.762+/−0.034>1

(f) $(|RL\rangle - |LR\rangle)/\sqrt{2}$

A\B	1	X	Y	Z
1		−0.059	−0.131	−0.015
X	0.066	−0.916	−0.167	−0.197
Y	0.105	0.089	−0.967	0.031
Z	−0.008	0.181	−0.093	−0.927

after filtering
−0.088	−0.175	0.339	B
0.015	0.151	−0.281	A

Σ 1.794+/−0.036>1
Σ 1.794+/−0.036>1

(g) $(|RR\rangle + |LL\rangle)/\sqrt{2}$

A\B	1	X	Y	Z
1		−0.058	0.115	0.001
X	0.076	−0.899	0.081	0.219
Y	−0.057	0.204	0.977	−0.069
Z	0.082	0.266	0.151	0.905

after filtering
−0.006	0.091	0.430	B
0.187	0.088	0.353	A

Σ 1.773+/−0.039>1
Σ 1.773+/−0.039>1

(h) $(|LL\rangle + i|RR\rangle)/\sqrt{2}$

A\B	1	X	Y	Z
1		0.028	0.005	−0.058
X	0.044	−0.017	−0.110	−0.959
Y	0.105	−0.014	0.978	−0.067
Z	−0.008	−0.954	−0.036	−0.056

after filtering
−0.029	−0.057	0.334	B
−0.290	−0.014	0.002	A

Σ 1.879+/−0.035>1
Σ 1.831+/−0.042>1

(i) $(|RR\rangle + i|LL\rangle)/\sqrt{2}$

A\B	1	X	Y	Z
1		0.051	0.051	0.055
X	0.133	0.082	0.929	0.204
Y	−0.034	0.964	0.069	0.007
Z	0.109	0.053	−0.159	0.962

after filtering
−0.029	0.056	0.522	B
0.058	0.014	0.557	A

Σ 1.859+/−0.051>1
Σ 1.859+/−0.051>1

(j) $(|HP\rangle + |VM\rangle)/\sqrt{2}$

A\B	1	X	Y	Z
1		0.021	0.015	−0.089
X	−0.092	0.110	0.098	0.952
Y	0.022	0.157	0.940	−0.041
Z	0.057	0.981	−0.007	−0.055

after filtering
−0.038	−0.013	0.340	B
0.295	−0.025	−0.054	A

Σ 1.792+/−0.033>1
Σ 1.868+/−0.031>1

FIG. 11. (Color online) Application of the decision tree on a selection of maximally entangled states, allowing one to determine the entanglement of the state by measuring the correlations marked in red. As an alternative, local filtering is applied in order to extract the correlations with maximal value (blue correlations).

[Fig. 12(c)], for which our method reveals entanglement after four steps, as the measurements of $T_{zz} = 0.007$, $T_{yy} = 0.069$, $T_{xx} = -0.801$, and $T_{yz} = -0.968$ give a value of $1.583 \pm 0.067 > 1$. Similarly, as expected, for a separable state such as $|HH\rangle$ [Fig. 12(f)], our entanglement criterion delivers a value of $\sum_{k,l=1}^{3} T_{kl}^2 = 0.964 \pm 0.062 < 1$ for measuring all correlations, not revealing entanglement clearly. These states, of course, can be analyzed also using Schmidt decomposition.

For maximally entangled states, the Bloch vectors after local filtering are also shown (blue color; see Fig. 11), while for nonmaximally entangled states (Fig. 12), no local filtering is required since the Bloch vectors are already nonvanishing. In all cases, only one entry of the respective Bloch vectors is large compared to the others. Therefore, no realignment of the analyzers is necessary. Due to Schmidt decomposition, the decision tree should start with a correlation measurement along

(a) $0.75|PP\rangle + 0.66i|MM\rangle$

A \ B	1	X	Y	Z
1		−0.090	0.087	0.367
X	−0.168	0.845	−0.068	−0.200
Y	−0.290	−0.221	−0.128	−0.911
Z	0.067	−0.077	−0.849	0.053

$\sum$ 1.563+/−0.061>1
$\sum$ 1.548+/−0.056>1

(b) $0.93|HH\rangle + 0.35|VV\rangle$

A \ B	1	X	Y	Z
1		−0.099	0.005	0.719
X	−0.083	0.649	0.031	−0.019
Y	0.128	−0.130	−0.618	0.160
Z	0.704	−0.062	−0.014	0.984

$\sum$ 1.350+/−0.041>1
$\sum$ 1.350+/−0.041>1

(c) $0.83|LH\rangle + 0.56i|RV\rangle$

A \ B	1	X	Y	Z
1		−0.075	−0.053	0.373
X	0.172	−0.801	0.037	0.357
Y	−0.393	−0.117	0.069	−0.968
Z	−0.036	−0.071	0.842	0.007

$\sum$ 1.583+/−0.053>1
$\sum$ 1.579+/−0.048>1

(d) $0.86|HH\rangle + 0.51|VV\rangle$

A \ B	1	X	Y	Z
1		0.029	−0.004	0.455
X	0.053	0.806	−0.008	0.052
Y	0.110	−0.114	−0.810	0.134
Z	0.441	−0.006	0.044	0.994

$\sum$ 1.644+/−0.053>1
$\sum$ 1.644+/−0.053>1

(e) $0.66|LM\rangle + 0.75|RP\rangle$

A \ B	1	X	Y	Z
1		0.349	−0.071	−0.108
X	0.104	0.069	−0.859	0.156
Y	−0.376	−0.976	0.118	−0.029
Z	−0.104	0.016	0.108	0.815

$\sum$ 1.631+/−0.043>1
$\sum$ 1.714+/−0.040>1

(f) $|HH\rangle$

A \ B	1	X	Y	Z
1		−0.027	−0.041	0.993
X	0.118	−0.022	0.028	0.128
Y	−0.001	−0.033	−0.042	0.039
Z	0.982	−0.027	−0.012	0.970

$\sum$ 0.964+/−0.062<1
$\sum$ 0.964+/−0.062<1

FIG. 12. (Color online) Application of the decision tree on a selection of nonmaximally entangled states, allowing one to determine the entanglement of the state by measuring the correlations marked in red. Due to the asymmetry of the states, local filtering is unnecessary, and the information on the Bloch vectors can be used to detect entanglement with a maximal number of three correlation measurements (blue correlations). (f) For a product state, the full set of correlations does not reveal entanglement, as it should be.

a direction in which we see a big local expectation value. In such a case, it is sufficient to cyclically relabel the required measurements as defined for the original decision tree. Following this method, it is possible to detect entanglement with a maximum number of three steps. The first correlation to be measured is determined by the Bloch vectors after applying local filtering.

2. Many qubits

For the demonstration of multiqubit entanglement detection, we use a family of three-photon polarization entangled Gdańsk (*G*) states [23] and the four-qubit Dicke state. The *G* states are defined by

$$|G(\alpha)\rangle = \cos(\alpha)|W\rangle + \sin(\alpha)|\overline{W}\rangle, \qquad (23)$$

where $|W\rangle = \frac{1}{\sqrt{3}}(|HHV\rangle + |HVH\rangle + |VHH\rangle)$, and in order to obtain $|\overline{W}\rangle$, one exchanges H and V. The four-qubit Dicke state with two "excitations" reads

$$
\begin{aligned}
\left|D_4^{(2)}\right\rangle = \frac{1}{\sqrt{6}}(&|HHVV\rangle + |HVHV\rangle + |VHHV\rangle \\
&+ |HVVH\rangle + |VHVH\rangle + |VVHH\rangle). \quad (24)
\end{aligned}
$$

Generalized three-qubit G state. In order to observe these states, a collinear type-II SPDC source together with a linear

setup to prepare the four-photon Dicke state $D_4^{(2)}$ is used [24,25]. The three-photon state is obtained if the first photon is measured to be $\cos(\alpha)|H\rangle + \sin(\alpha)|V\rangle$ polarized.

The protocol for entanglement detection starts with observers locally measuring the polarization of their respective photons, enabling them to individually determine the Bloch vectors.

(i) For the $G(\pi/4)$ state, we obtain $T_{i00} = (0.636, -0.008, -0.015)$, $T_{0j0} = (0.623, -0.092, 0.010)$, and $T_{00k} = (0.636, 0.070, 0.022)$. The Bloch vectors suggest that the correlation T_{xxx} is big. Therefore, the decision tree starts with the measurement of $T_{xxx} = 0.904 \pm 0.025$ and continues with $T_{xzz} = -0.578 \pm 0.025$ (see Fig. 3). These two measurements already prove entanglement because $T_{xxx}^2 + T_{xzz}^2 = 1.152 \pm 0.038 > 1$.

(ii) For the *W* state, $G(\pi/2)$, the Bloch vectors are $T_{i00} = (0.016, -0.070, 0.318)$, $T_{0j0} = (-0.010, -0.073, 0.308)$, and $T_{00k} = (-0.011, -0.0547, 0.319)$, which suggests that now the correlation T_{zzz} is big. Indeed, we observe $T_{zzz} = -0.882 \pm 0.025$. The decision tree is the same as above, but with local axes renamed as follows: $x \to z \to y \to x$. Therefore, the second measurement has to be T_{zyy}. With $T_{zyy} = 0.571 \pm 0.025$, we again prove entanglement as $T_{xxx}^2 + T_{zyy}^2 = 1.104 \pm 0.037 > 1$.

Four-qubit Dicke state. Here, we have vanishing Bloch vectors, $T_{i000} = (-0.020, -0.016, 0.007)$, $T_{0j00} = (-0.011, -0.029, 0.014)$, $T_{00k0} = (-0.018, -0.020, -0.004)$, and $T_{000l} = (-0.009, -0.022, 0.008)$. We construct a set of mutually commuting operators, which form the first branch of the four-qubit decision tree starting with $T_{zzzz}\{zzzz \rightarrow zzxx \rightarrow zxzx \rightarrow zxxz \rightarrow xzxz \rightarrow xxzz \rightarrow xzzx \rightarrow xxxx \rightarrow yyyy\}$. After measuring the correlations, $T_{zzzz} = 0.848 \pm 0.025$, $T_{zzxx} = -0.533 \pm 0.025$, $T_{zxzx} = -0.552 \pm 0.025$, our algorithm succeeds since $T_{zzzz}^2 + T_{zzxx}^2 + T_{zxzx}^2 = 1.3082 \pm 0.041 > 1$.

VI. CONCLUSIONS

The entanglement of arbitrary multiqubit states can be efficiently detected based on two methods described here. Both methods employ a criterion based on the sum of squared correlations. Combining this with an adaptive determination of the correlations to be measured allows one to succeed much faster than standard tomographic schemes. The first one, particularly designed for two-qubit states, determines the Schmidt decomposition from local measurements only, where at most three correlation measurements are sufficient for entanglement detection. The second one employs a decision tree to speed up the analysis. Its design is based on correlation complementarity and prevents one from measuring less informative correlations. The performance of the scheme is numerically analyzed for arbitrary pure states and, in the two-qubit case, for mixed states. The schemes succeed, on average, at least one step earlier as compared with random sampling on two-qubit states, with an exponentially increasing speedup for a higher number of qubits. Our results encourage the application of these schemes in state-of-the-art experiments with quantum states of increasing complexity.

[1] R. Horodecki, P. Horodecki, M. Horodecki, and K. Horodecki, Rev. Mod. Phys. **81**, 865 (2009).

[2] J.-W. Pan, Z.-B. Chen, C.-Y. Lu, H. Weinfurter, A. Zeilinger, and M. Żukowski, Rev. Mod. Phys. **84**, 777 (2012).

[3] M. A. Nielsen and I. Chuang, *Quantum Computation and Quantum Information* (Cambridge University Press, New York, 2000).

[4] M. Horodecki, P. Horodecki, and R. Horodecki, Phys. Lett. A **223**, 1 (1996).

[5] M. Bourennane, M. Eibl, C. Kurtsiefer, S. Gaertner, H. Weinfurter, O. Gühne, P. Hyllus, D. Bruß, M. Lewenstein, and A. Sanpera, Phys. Rev. Lett. **92**, 087902 (2004).

[6] B. M. Terhal, Phys. Lett. A **271**, 319 (2000).

[7] M. Lewenstein, B. Kraus, J. I. Cirac, and P. Horodecki, Phys. Rev. A **62**, 052310 (2000).

[8] D. Bruß, J. I. Cirac, P. Horodecki, F. Hulpke, B. Kraus, M. Lewenstein, and A. Sanpera, J. Mod. Opt. **49**, 1399 (2002).

[9] O. Gühne and P. Hyllus, Int. J. Theor. Phys. **42**, 1001 (2003).

[10] O. Gühne and G. Toth, Phys. Rep. **474**, 1 (2009).

[11] P. Badziąg, Č. Brukner, W. Laskowski, T. Paterek, and M. Żukowski, Phys. Rev. Lett. **100**, 140403 (2008).

[12] W. Laskowski, D. Richart, C. Schwemmer, T. Paterek, and H. Weinfurter, Phys. Rev. Lett. **108**, 240501 (2012).

[13] P. Kurzyński, T. Paterek, R. Ramanathan, W. Laskowski, and D. Kaszlikowski, Phys. Rev. Lett. **106**, 180402 (2011).

[14] E. Schmidt, Math. Ann. **63**, 433 (1906).

[15] A. Peres, *Quantum Theory: Concepts and Methods* (Kluwer Academic, Dordrecht, 1995).

[16] G. Toth and O. Gühne, Phys. Rev. A **72**, 022340 (2005).

[17] S. Wehner and A. Winter, J. Math. Phys. **49**, 062105 (2008).

[18] S. Wehner and A. Winter, New J. Phys. **12**, 025009 (2010).

[19] G. Vidal and R. F. Werner, Phys. Rev. A **65**, 032314 (2002).

[20] R. F. Werner, Phys. Rev. A **40**, 4277 (1989).

[21] P. G. Kwiat, E. Waks, A. G. White, I. Appelbaum, and P. H. Eberhard, Phys. Rev. A **60**, R773 (1999).

[22] P. Trojek and H. Weinfurter, Appl. Phys. Lett. **92**, 211103 (2008).

[23] A. Sen(De), U. Sen, and M. Żukowski, Phys. Rev. A **68**, 032309 (2003).

[24] R. Krischek, C. Schwemmer, W. Wieczorek, H. Weinfurter, P. Hyllus, L. Pezze, and A. Smerzi, Phys. Rev. Lett. **107**, 080504 (2011).

[25] N. Kiesel, C. Schmid, G. Tóth, E. Solano, and H. Weinfurter, Phys. Rev. Lett. **98**, 063604 (2007).